Laser transition probabilities in Xe I

Arati Dasgupta* and J. P. Apruzese
Plasma Physics Division, Naval Research Laboratory, Washington, DC 20375, USA

Oleg Zatsarinny† and Klaus Bartschat
Department of Physics and Astronomy, Drake University, Des Moines, Iowa 50311, USA

Charlotte Froese Fischer‡
National Institute of Standards and Technology, Gaithersburg, Maryland 20899, USA

The atomic xenon laser is among the most efficient and powerful of the near-infrared gas lasers, especially when pumped by molecular ions in an Ar-Xe mixture. Accurate transition probabilities for the laser transitions are critical in developing a fundamental understanding of the inversion dynamics, gain, and power extraction of this device. We compare results from several methods of calculating transition probabilities for six laser lines ranging in wavelength from 1.733 to 3.508 μm. In some cases, our recommended values differ considerably from those employed in previous work.

I. INTRODUCTION

Lasing in atomic xenon was first demonstrated by Patel and co-workers in 1962 [1], at a wavelength of 2.027 μm. Since then, this laser has been intensively investigated by many researchers in several countries [2–16]. It has been found that its highest efficiency is attained by mixing the Xe with Ar, requiring about two orders of magnitude more Ar to be present than Xe. The maximum in both efficiency and power occurs when the $5d[3/2]_1 \rightarrow 6p[5/2]_2$ (1.733 μm) transition [17] is the principal laser line. Altogether, lasing has been observed on at least six transitions, which are listed in Table I below. The relative strengths of these lines as components of the atomic Xe laser exhibit interesting variations with respect to the Xe concentration, the identity of the gas with which Xe is mixed, pump power, and pressure. Interested readers should consult the above-cited references for further details, particularly Ref. [5].

Much of the work subsequent to the initial lasing demonstration has focused on resolving key physics issues regarding the mechanism of population inversion [4–13], demonstrating high single-pulse laser yield [14], and achieving quasicontinuous wave (cw) operation by employing a repetitively pulsed generator to drive the laser [15]. A recent review was published by Kholin [16]. Though there is general agreement that the dissociative recombination of ArXe⁺ is an important source of the population inversions, the potentially significant role of Xe_2^+ in that regard is less clear. Some have suggested that Xe_2^+ is either unimportant or populates the lower laser levels [2,3,7,9,11,13] while others [5,6,8,10,12,14] maintain that it is a significant driver of the gain.

Continued confrontation and feedback between models and experimental as well as theoretical data is critical to resolving the basic physics issues concerning the laser's inversion kinetics as well as further practical improvements in its operation. One of the most basic elements of any such model is the set of transition probabilities which characterize the laser transitions. For each laser line, the gain is proportional to the transition probability, and inversely proportional to the saturation intensity. In modeling the atomic xenon laser, the transition probabilities obtained by Allen, Jones, and Schofield [18] or by Aymar and Coulombe [19] are frequently incorporated. In the present work, we compare several methods of calculating the transition probabilities which in some cases differ significantly from those of Refs. [18] and/or [19].

II. COMPUTATIONAL METHODS

Below we briefly describe several numerical methods, which were used to calculate the energy levels and the relevant transition probabilities for the present work. The radiative transition probability from level $|j\rangle$ to a lower level $|k\rangle$ can be written as

$$A_{jk}^r = [32\pi^3\sigma_{jk}^3/3c^3(2J_j+1)]|\langle\gamma_k J_k||D||\gamma_j J_j\rangle|^2, \qquad (1)$$

where γ is used to designate all quantum numbers other than the total electronic angular momentum J. Furthermore, D is

TABLE I. Transition energies (in cm⁻¹) for six principal infrared laser transitions from $5p^56p$ to $5p^55d$ levels in Xe I. The experimental level splittings [17] are compared with results from the *ab initio* structure models.

Transition	ΔE [17]	MCDHF	BSR
$5d[3/2]_1 - 6p[5/2]_2$	5770	5836	5483
$5d[3/2]_1 - 6p[3/2]_1$	4934	5036	4926
$5d[5/2]_2 - 6p[5/2]_2$	3806	3323	3426
$5d[3/2]_1 - 6p[1/2]_0$	3771	3775	3512
$5d[5/2]_2 - 6p[3/2]_1$	2969	2523	2869
$5d[7/2]_3 - 6p[5/2]_2$	2851	2404	2480

*Electronic address: dasgupta@ppdmail.nrl.navy.mil
†Electronic address: oleg_zoi@yahoo.com
‡Electronic address: charlotte.fischer@nist.gov

the electric dipole operator for the electromagnetic interaction and σ_{jk} is the wavenumber (in cm^{-1}). Unless indicated otherwise, atomic units are used throughout.

A. Modified relativistic Hartree-Fock-Slater method (MRHFS)

We have employed a modified version of Slater's $X\alpha$ self-consistent method, which is also known as the Hartree-Fock-Slater (HFS) procedure in calculating the wave functions of the outer electrons. The bound orbitals of the core up to the $5s$ orbital for this calculation were obtained by using the parameters given by Clementi and Roetti [20]. For the outermost $5p$ and the excited $6p$ and $5d$ orbitals we employed a semiempirical approximation, which is described in detail in [21,22]. The radial part of the bound orbital P_{nl} in this method is obtained by solving the equation

$$\left[\frac{d^2}{dr^2} - \frac{l(l+1)}{r^2} - 2V_0(r) - 2\beta V_{ex}(r) - 2V_D(r) - 2V_{mv}(r) \right.$$
$$\left. - E_{nl} \right] P_{nl}(r) = - \sum_{n' < n} \mu_{n'l} P_{n'l}(r). \quad (2)$$

Here $V_0(r)$ and $V_{ex}(r)$ are the Coulomb and the static-exchange potentials of the ionic core. They can be expressed as

$$V_0 = -\frac{Z_n}{r} + \sum_i w_i \left[\frac{1}{r} \int_0^r P_i^2(t)dt + \int_r^\infty \frac{1}{t} P_i^2(t)dt \right] \quad (3)$$

and

$$V_{ex}(r) = -\frac{1}{2} \left[\frac{81}{4\pi^2 r^2} \sum_i w_i P_i^2(r) \right]^{1/3}, \quad (4)$$

where the P_i are the radial orbitals of the inner electrons in subshell "i," w_i is the number of electrons in the subshell, and Z_n is the nuclear charge. The sum on the right-hand side of Eq. (2), involving the Lagrange multipliers $\mu_{n'l}$, ensures that P_{nl} is orthogonal to the other bound orbitals with the same angular momentum l. Furthermore, $V_D(r)$ and $V_{mv}(r)$ are the relativistic Darwin and mass-velocity terms, respectively. The radial functions P_{nl} are obtained by solving Eq. (2) using the spherically symmetric potential of the charge distribution for each level and varying the parameter β to obtain the experimental ionization energy E_{nl} for the fine-structure level of interest. This method is similar to the HFS procedure, except that only the contributions of the *inner* electrons but not of P_{nl} are included in the summations for V_0 and V_{ex}. This omission not only simplifies the calculation, but it also automatically leads to the correct asymptotic form of the potential V_0. In the HFS procedure, the constant E_{nl} is determined from a variational approach by solving the radial equation, whereas we use the experimental binding energy value for E_{nl} and vary β. This method emphasizes the behavior of the outer part of P_{nl} which is usually most important for transition probability calculations.

The radial wave functions for the $5p^56p$ and $5p^55d$ levels were calculated by using the experimental binding energy for each individual fine-structure level. For each level, we generate the relevant F and G integrals, as well as the spin-orbit parameter ζ_{nl} from the term-averaged wave functions P_{nl}. Using an intermediate angular-momentum coupling scheme, each mixed level for a given angular momentum J is expressed as

$$|\alpha J\rangle = \sum_{SL} C_{\alpha SLJ} |\alpha SLJ\rangle \quad (5)$$

within the same configuration α. For mixing among the LS terms with the same parity and total angular momentum, J, the mixing coefficients $C_{\alpha SLJ}$ are obtained by diagonalizing the spin-orbit Hamiltonian with level specific F, G, and ζ_{nl} for each J. The transition probabilities are then calculated for the desired transitions.

B. Multiconfiguration Dirac-Hartree-Fock calculations (MCDHF)

The theoretical basis of this computation is the multiconfiguration Dirac-Hartree-Fock (MCDHF) method [23] together with the core-valence (CV) correlation model. This model proved to be very effective for computing $2p^4(^3P)3p - 2p^4(^3P)3d$ transitions in Ne II [24,25]. It generally works well for transitions between excited states, if both states have the same LS parent configuration. In Xe, this parent is $[\text{Kr}]4d^{10}5s^25p^5~^2P_{3/2}^o$. We use nonrelativistic notation and do not specify the J values for the sake of brevity, although the calculations were properly carried out using fully relativistic terms. An inactive $[\text{Kr}]4d^{10}$ core is assumed and the problem is treated as a $5s^25p^56p - 5s^25p^55d$ transition. The CV model does not accurately predict the energy of the ground state relative to the excited states and, therefore, any interaction with this even-parity $J=0$ state (the ground state) will be very approximate.

In the MCDHF procedure, the wave function Ψ for the state labeled γJ is approximated by an expansion over jj-coupled configuration state functions (CSFs)

$$\Psi(\gamma J) = \sum_j c_j \Phi(\gamma_j J), \quad (6)$$

where the CSFs $\Phi(\gamma J)$ are antisymmetrized linear combinations of relativistic orbital products of the form

$$\phi(\mathbf{r}) = \frac{1}{r} \begin{pmatrix} P_{n\kappa}(r)\chi_{\kappa m}(\hat{r}) \\ iQ_{n\kappa}(r)\chi_{-\kappa m}(\hat{r}) \end{pmatrix}. \quad (7)$$

Here κ is the relativistic angular momentum, $P_{n\kappa}(r)$ and $Q_{n\kappa}(r)$ are the large and small component radial wave functions, and $\chi_{\kappa m}(\hat{r})$ is the spinor spherical harmonic in the lsj coupling scheme. Transition calculations between separately optimized wave functions were computed using biorthogonal transformations [26].

In the core-polarization model, the wave function is an expansion over the set of either odd or even configuration states $5s^25p^4nln'l'$ and $5s5p^5nln'l'$, where nl and $n'l'$ are members of an orbital set. In our work, the $1s, 2s, 2p, \ldots, 4d$ orbitals for the parent states were determined from extended optimal level (EOL) calculations for $5s^25p^56p$ or $5s^25p^55d$ and the selected J. The $1s, 2s, 2p, \ldots, 5p$ orbitals were then

TABLE II. Wavelengths (μm) and transition probabilities (s^{-1}) of six principal infrared laser transitions from $5p^56p$ to $5p^55d$ levels in Xe I. The notation x.xx(+n) is used to denote x.xx $\times$ 10^n, and the superscript L (V) refers to the results obtained with the length (velocity) form of the electric dipole operator. All theoretical results were rescaled using the experimental level splittings [17].

	NIST [17]	MRHFS	MCDHF		BSR		Ref. [19]		Recommended
Transition	λ	A_{ki}^L	A_{ki}^L	A_{ki}^V	A_{ki}^L	A_{ki}^V	A_{ki}^L	A_{ki}^V	Value
$5d[3/2]_1 - 6p[5/2]_2$	1.733	4.61(+5)	3.94(+5)	3.96(+5)	5.81(+5)	5.42(+5)	3.05(+5)	1.57(+5)	4.8$\pm$.9(+5)
$5d[3/2]_1 - 6p[3/2]_1$	2.027	2.24(+6)	2.39(+6)	5.72(+5)	2.57(+6)	2.93(+6)	2.46(+6)	1.15(+6)	2.4$\pm$.2(+6)
$5d[5/2]_2 - 6p[5/2]_2$	2.628	5.95(+5)	5.87(+5)	4.07(+5)	6.90(+5)	1.09(+6)	7.42(+5)	5.29(+5)	6.2$\pm$.5(+5)
$5d[3/2]_1 - 6p[1/2]_0$	2.652	1.69(+6)	1.38(+6)	3.76(+5)	1.77(+6)	1.73(+6)	1.27(+6)	9.30(+5)	1.6$\pm$.2(+5)
$5d[5/2]_2 - 6p[3/2]_1$	3.368	5.87(+5)	5.48(+5)	5.65(+5)	6.30(+5)	8.68(+5)	6.81(+5)	7.22(+5)	5.9$\pm$.4(+5)
$5d[7/2]_3 - 6p[5/2]_2$	3.508	5.59(+5)	5.84(+5)	4.74(+5)	6.90(+5)	1.05(+6)	7.37(+5)	7.68(+5)	6.1$\pm$.7(+5)

kept fixed in calculations that included correlation. The first calculation for each state of interest had expansions over the set of orbitals $5d, 5f, 5g, 6s, 6p, 6d, 6f, 6g$. (Since the principal quantum number is not important for correlation orbitals, it was convenient to treat $4f$ as inactive.) If the state of interest was not the lowest in energy, the $5d, 5f, 5g$ orbitals (for even parity) and the $5f, 5g, 6s$ orbitals (for odd parity) were optimized on the lower states in order to define a reasonable spectrum, whereas the remaining $n=6$ orbitals were optimized on the excited state of interest. The expansions were then extended to also include $7s, 7p,$ and $7d$ orbitals optimized on the specific state of interest. The Breit correction was not significant and the transition probabilities were obtained in the Dirac-Coulomb approximation.

C. Multi-channel B-spline R-matrix (BSR) calculations

The calculations of Xe bound states are complicated by several factors. First, the valence orbitals in the $5p^5nl$ configurations exhibit a strong term dependence, particularly in the $5p^5nd^{1,3}P$ and $5p^5np^{1,3}S$ states. Second, due to the unfilled $5p$ shell, there is a strong spin-orbit mixing of different terms. Further complication arises from strong configuration mixing between the $5p^5(n+1)s$ and $5p^5nd$ series. These effects can be directly accounted for by employing the B-spline box-based multichannel method described by Zatsarinny and Froese Fischer [27].

In this method, the atomic wave function describing the total ($N+1$)-electron system is expanded in terms of products of the N-electron target states and the radial functions for the outer electron, which in turn are expanded in a B-spline basis. In the present calculation of the Xe Rydberg series, the corresponding close-coupling expansion had the structure

$$\Phi(5s^25p^5nl; J\pi) = A\sum_{i,j} c_{ij}\varphi(5s^25p^5; {}^2P)B_i(r)|l_js\rangle$$
$$+ A\sum_{i,j} c_{ij}\varphi(5s5p^6; {}^2S)B_i(r)|l_js\rangle$$
$$+ A\sum_{i,j,LS} c_{ij}\varphi(5s^25p^45d; LS)B_i(r)|l_js\rangle$$
$$+ A\sum_{i,j,LS} c_{ij}\varphi(5s^25p^46s; LS)B_i(r)|l_js\rangle.$$

$$(8)$$

Here the B-splines $B_i(r)$ represent the radial part of the valence orbitals and $|l_js\rangle$ denotes the spin-angular part of the one-electron functions. The operator A includes antisymmetrization and implies that the target function φ is coupled to the valence electron, according to the usual angular-momentum rules, to form a state with total electronic angular momentum J and parity π. The choice of B-splines as basis functions has some advantages. A detailed discussion of B-splines and their application in atomic structure calculations can be found in the review of Bachau *et al.* [29]. The expansion coefficients c_{ij} for each given set of (J, π) are found by diagonalizing the atomic Hamiltonian inside a box of radius a. In the B-spline basis, this leads to a generalized eigenvalue problem of the form

$$Hc = ESc, \qquad (9)$$

where S is the overlap matrix. If the usual orthogonal conditions are imposed on the channel orbitals, it reduces to a banded matrix, consisting of overlaps between individual B splines. In the more general case of nonorthogonal orbitals used in the present calculations, a detailed description of the structure of the H and S matrices in the B-spline representation was given by Zatsarinny and Froese Fischer [28]. The boundary conditions are imposed by deleting from the expansion the first and last splines, i.e., the only splines which have a nonzero value at the boundaries $r=0$ and $r=a$. In the present calculations, the atomic Hamiltonian H includes all one-electron Breit-Pauli operators plus the two-electron spin-other-orbit interaction. Therefore, our B-spline expansions for the Rydberg orbitals (and hence the radial functions for the outer electron) *directly* include relativistic corrections.

The correlation corrections in the excited Xe states are primarily due to the core-valence interaction. The importance of the latter interaction manifests itself in the Hartree-Fock (HF) binding energies of the lowest states, which differ from the experimental values by approximately (0.25, 0.35, and 0.15) eV for the $5p^55d$, $5p^56s$, and $5p^56p$ states, respectively. The core-valence correlation was introduced in the present calculations by using excited target states in the close-coupling expansion (8), where the last three terms are included to simulate the core-valence correlation for the $5p^5nl$ states represented by the first term. The 6s and 5d orbitals in the third and fourth terms were obtained from HF calculations for the corresponding target states in Xe$^+$. Alto-
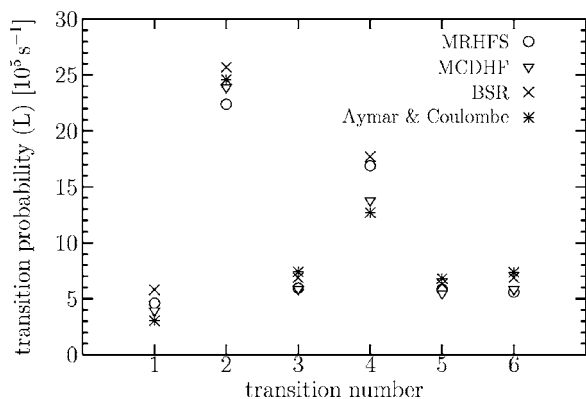
FIG. 1. Length-form results of the transition probabilities from the various methods listed in Table II. The transition number corresponds to the row number in the table.

gether, our CC expansion (8) included 18 LS target states, and we restricted our consideration to the ns, np, nd, and nf Rydberg series. This resulted in up to 67 channels and a maximum rank of 3685 of the interaction matrix. Using this expansion, we managed to reduce the errors in the binding energies to 0.1 eV or less.

It was generally thought that the inner-core correlation only has a small influence on the valence orbitals and, therefore, the frozen HF $5p^5$ core would be a good approximation for all excited states. As shown in recent MCHF calculations by Irimia and Froese Fischer [30], however, the core correlation is also important for an accurate calculation of the transition probabilities in Ar, and a similar importance can be expected for the Xe case. In the present calculations, the inner-core correlation was taken into account by using extensive multiconfiguration expansions for the $5s^2 5p^5$ core state, obtained by single and double promotion of the $5s$ and $5p$ orbitals to $\bar{6}l$ correlated orbitals. (The $1s$-$4d$ subshells were treated as an inert core, and we use a bar over the principal quantum number to indicate a correlation orbital.) The main contributions originate from the $5s 5p^5 \bar{6}d$, $5s 5p^4 \bar{6}d^2$, and $5s 5p^5 \bar{6}f$ configurations. Another important parameter is the spin-orbit splitting of the $5p^5$ core. This parameter is a dominant factor in the spin-orbit mixing of different terms in the excited states. The nonrelativistic HF core orbitals do not include the relativistic contraction of the one-electron orbitals and, therefore, underestimate the spin-orbit interaction. In order to reproduce the experimental value for the $^2P_{3/2} - ^2P_{1/2}$ core splitting, we multiplied the $\zeta(5p)$ spin-orbit parameter by 1.215.

The number of physical states that we can generate by this method depends on the radius a of the B-spline box. Our choice of $a = 300 a_0$ (with a_0 denoting the Bohr radius) yields a good description for all spectroscopic states $5s^2 5p^5 nl$ up to $n = 10$. We used B-splines of order 8 with an exponential grid of knots that required 55 B-splines to cover the entire region under consideration. We emphasize again that the above procedure generates nonorthogonal, term-dependent radial functions for each individual ($5s^2 5p^5 nl \ LSJ\pi$) state, also accounting for term mixing due to the spin-orbit interaction. All calculations were performed with the recently published B-spline code BSR [31].

III. RESULTS AND DISCUSSION

In variational, *ab initio* methods such as MCDHF and BSR, the wave functions that are used in the transition probability calculation are optimized on the energy. One check on the adequacy of the wave functions is the theoretical transition energy. Table I compares these energies (in cm^{-1}) with the National Institute of Standards and Technology (NIST) values compiled from observation [17]. For some transitions, the agreement is within a few percent, whereas for others the difference is as large as 15%.

The results for the transition probabilities obtained from the various methods described above are summarized in Table II. All have been rescaled to the observed wavelengths. For the *ab initio* methods, results obtained in both the length and velocity forms of the electric dipole operator are provided. Though agreement in the two gauges is desirable, it is not a direct check on accuracy. Among the methods used in this work, the BSR model is the only one currently accounting for both core-valence and inner-core correlation, and this may explain the relatively good overall agreement between the results obtained in the two gauges. On the other hand, the Breit-Pauli approximation is a low-order relativistic theory for the wave function. The transition operator in the velocity form has omitted some low-order corrections that are particularly important for transitions between states with different total spin [32,33] or, as in the present case, between components of the wave function with different total spin. Note that all states involved in the transitions of interest have highly mixed singlet and triplet components.

No such corrections are needed in the length form. This form is also preferred for MCDHF calculations, where results from the length form have been shown to be in better agreement with experiment [34]. Figure 1 shows the spread of the length-form results from all methods for the six transitions considered in this work. In the absence of both direct experimental data and even more elaborate calculations, which are nontrivial and should ideally be performed in a fully relativistic framework including extensive correlation in the description of the $5p^6$, $5p^5 6s$, $5p^5 6p$, and $5p^5 5d$ levels, it is difficult to judge which of the current results is most reliable. However, we believe that the average of the present length values is to be preferred over the values currently used in the literature, and that the spread in the individual results can serve as an indicator of the uncertainty. These have been included in Table II as recommended values.

IV. CONCLUSIONS

In the present work, semiempirical relativistic Hartree-Fock-Slater calculations are reported for six transitions in Xe and checked with *ab initio* Breit-Pauli and multiconfiguration Dirac-Hartree-Fock theories that included selected correlation effects. All these results agree in that the transition rate for the most important 1.733 μm transition is significantly larger $(3.9 \times 10^5 - 5.8 \times 10^5)$/s than the 3.05×10^5/s reported earlier by Aymar and Coulombe [19]. For other transitions there is more variation, with MRHFS agreeing with either BSR or MCDHF within 7%.

[1] C. K. N. Patel, W. L. Faust, and R. A. McFarlane, Appl. Phys. Lett. **1**, 84 (1962).

[2] N. G. Basov, V. V. Baranov, A. Y. Chugunov, V. A. Danilychev, A. Y. Dudin, I. V. Kholin, N. N. Ustinovskii, and D. A. Zayarnyi, IEEE J. Quantum Electron. **21**, 1756 (1985).

[3] N. G. Basov, V. V. Baranov, V. A. Danilychev, A. Y. Dudin, D. A. Zayarnyi, A. V. Rzhevskii, N. N. Ustinovskii, I. V. Kholin, and A. Y. Chugunov, Sov. J. Quantum Electron. **16**, 1008 (1986).

[4] P. J. M. Peters, Q.-C. Mei, and W. J. Witteman, Appl. Phys. Lett. **54**, 193 (1989).

[5] M. Ohwa, T. J. Moratz, and M. J. Kushner, J. Appl. Phys. **66**, 5131 (1989).

[6] A. Suda, B. L. Wexler, K. J. Riley, and B. J. Feldman, IEEE J. Quantum Electron. **26**, 911 (1990).

[7] P. J. Peters, Y. F. Lan, M. Ohwa, and M. J. Kushner, IEEE J. Quantum Electron. **26**, 1964 (1990).

[8] D. A. Zayarnyi, A. G. Korolev, N. N. Sazhina, N. N. Ustinovskii, and I. V. Kholin, Sov. J. Quantum Electron. **21**, 488 (1991).

[9] A. Y. Dudin, D. A. Zayarnyi, L. V. Semenova, N. N. Ustinovskii, I. V. Kholin, and A. Y. Chugunov, Quantum Electron. **23**, 578 (1993).

[10] T. T. Perkins, J. Appl. Phys. **74**, 4860 (1993).

[11] O. V. Sereda, V. F. Tarasenko, A. V. Fedenev, and S. I. Yakovlenko, Quantum Electron. **23**, 459 (1993).

[12] A. V. Karelin and O. V. Simakova, Quantum Electron. **34**, 29 (2004).

[13] S. W. A. Gielkens, W. J. Witteman, V. N. Tskhai, and P. J. M. Peters, IEEE J. Quantum Electron. **34**, 250 (1998).

[14] L. N. Litzenberger, D. W. Trainor, and M. W. McGeoch, IEEE J. Quantum Electron. **26**, 1668 (1990).

[15] S. B. Alexeev, N. N. Koval, V. M. Orlovskii, V. S. Skakun, V. F. Tarasenko, V. S. Tolkachev, A. V. Fedenev, M. A. Shulepov, and P. M. Shchanin, Quantum Electron. **34**, 519 (2004).

[16] I. V. Kholin, Quantum Electron. **33**, 129 (2003).

[17] E. B. Saloman, J. Phys. Chem. Ref. Data **33**, 765 (2004); (http://physics.nist.gov/PhysRefData/ASD/).

[18] L. Allen, D. G. C. Jones, and D. G. Schofield, J. Opt. Soc. Am. **59**, 842 (1969).

[19] M. Aymar and M. Coulombe, At. Data Nucl. Data Tables **21**, 537 (1978).

[20] E. Clementi and C. Roetti, At. Data Nucl. Data Tables **14**, 177 (1974).

[21] A. Dasgupta, M. Blaha, and J. L. Giuliani, Phys. Rev. A **61**, 012703 (2000).

[22] A. Dasgupta, K. Bartschat, D. Vaid, A. N. Grum-Grzhimailo, D. H. Madison, M. Blaha, and J. L. Giuliani, Phys. Rev. A **64**, 052710 (2001).

[23] F. A. Parpia, C. Froese Fischer, and I. P. Grant, Comput. Phys. Commun. **94**, 249 (1996).

[24] C. Froese Fischer and X. He, Can. J. Phys. **77**, 177 (1999).

[25] C. Froese Fischer and P. Jönsson, J. Mol. Struct. **537**, 55 (2001).

[26] J. Olsen, M. R. Godefroid, P. Jönsson, P. Å. Malmqvist, and C. Froese Fischer, Phys. Rev. E **52**, 4499 (1995).

[27] O. Zatsarinny and C. F. Fischer, J. Phys. B **35**, 4669 (2002).

[28] O. Zatsarinny and C. Froese Fischer, J. Phys. B **33**, 313 (2000).

[29] H. Bachau, E. Cormier, P. Decleva, J. E. Hansen, and F. Martin, Rep. Prog. Phys. **64**, 1815 (2001).

[30] A. Irimia and C. Froese Fischer, J. Phys. B **37**, 1659 (2004).

[31] O. Zatsarinny, Comput. Phys. Commun. **174**, 273 (2006).

[32] G. W. F. Drake, Phys. Rev. A **5**, 1979 (1972).

[33] Z. B. Rudzikas, J. M. Kaniauskas, G. V. Merkelis, and E. H. Savicius, J. Phys. B **16**, 2879 (1983).

[34] P. Jönsson, C. Froese Fischer, and E. Träbert, J. Phys. B **31**, 3497 (1998).